

Complexation of Gadolinium(III) and terbium(III) with nalidixic acid (NDX): Molar conductivity, thermal and spectral investigation

Ahmed I. El-Shenawy^{1,2,*}, Aly H. Atta^{1,3}, and Moamen S. Refat^{4,5}

¹Department of Chemistry, Faculty of Science, Dammam University, Kingdom Saudi Arabia

²Department of Chemistry, Faculty of Science, Benha University, Egypt

³Department of Chemistry, Faculty of Science, Suez University, Suez, Egypt

⁴Department of Chemistry, Faculty of Science, Taif University, Al-Hawiah, Taif, P.O. Box 888 Zip Code 21974, Saudi Arabia

⁵Department of Chemistry, Faculty of Science, Port Said University, Port Said, Egypt

*E-mail: aielshenawy@gmail.com

Received: 26 February 2014 / Accepted: 7 May 2014 / Published: 16 June 2014

The goal of this paper is recognized to the chemical and microbial impact resulting from the interaction between nalidixic acid (NDX) and two lanthanide salts ($GdCl_3 \cdot 6H_2O$ and $TbCl_3 \cdot 6H_2O$), which were prepared in normal and nano-scale range. Gadolinium and terbium(III) metal ions chelated with NDX through the deprotonation of carboxylic group of NDX bidentate ligand and oxygen atom of carbonyl group. The analytical analyses (elemental analyses, electrical conductivity) and spectroscopic measurements (FT-IR spectral, X-ray powder diffraction (XRD) and scanning electron microscopy (SEM)) as well as thermal analysis (TG/DTA) have been used to characterize the new solid complexes. The stability of NDX complexes was checked using Coats-Redfern and Horowitz-Metzger integral methods for the main thermal decomposition steps in the TG curves. The shiny side in this paper is focused on the preparation and characterization of single phases of gadolinium and terbium(III) oxide nanoparticles using carbamide as precursors. The NDX ligand in comparison with both cases traditional and nano-particles lanthanide complexes were assessment against for some kind of bacteria (*Escherichia Coli*, *Staphylococcus Aureus*, *Bacillus subtilis* and *Pseudomonas aeruginosa*) and fungi (*Aspergillus Flavus* and *Candida Albicans*) activities. The highest antibacterial and antifungal activities data of the nano-particles complexes were observed with more potent than the free NDX and traditional lanthanide complexes.

Keywords: Nalidixic acid; Nano-scale; Gadolinium; Terbium; Molar conductance; Optical investigation.

1. INTRODUCTION

Study of the interaction between drugs and metal ions is an important and active research area in bioinorganic chemistry [1-4]. It is well known that the action of many drugs is dependent on the coordination with metal ions [1] or the inhibition [2] on the formation of metalloenzymes. Quinolones considered a class of antibacterial agents which have been known for over 40 years [5]. Presence of metal ions considerably alters the activity of quinolones against potentially susceptible bacteria [6]. The interaction of metal ions with diverse deprotonated quinolones as ligands has been thoroughly discussed [7-16]. Quinolones have been classified in generations based on their activity [17]. Each generation presents an enhanced spectrum of activity in comparison to a previous one. Nalidixic acid (Fig. 1) is an example of first-generation quinolones that are active against Gram-negative organisms and they are used for the treatment of uncomplicated urinary tract infections [18]. The association complexes resulted between nalidixic acid and different metal ions has been described [19-25]. The copper and calcium(II) nalidixic acid complexes have been studied [19]. Nakano *et al.* [22] studied the corresponding complexes of nalidixic acid with Al^{3+} , Mg^{2+} and Ca^{2+} . Therefore, the importance of this paper is to study the physical and chemical structural of the interaction between the gadolinium or terbium(III) ions with NDX antibiotic ligand in nano-structural fashion. The coordination mode of nalidixic acid chelation has been investigated.

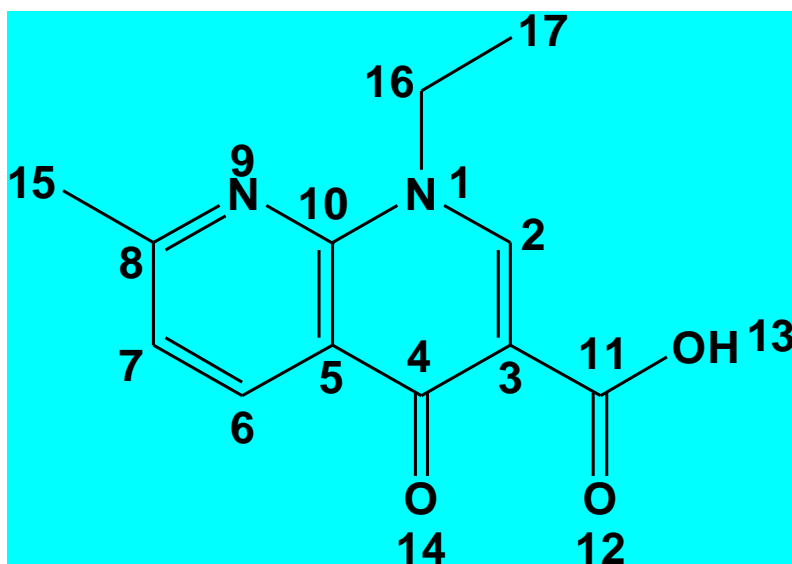


Figure 1. The structural formula of nalidixic acid (NDX)

2. EXPERIMENTAL

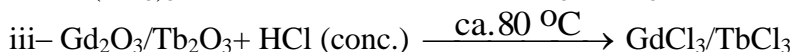
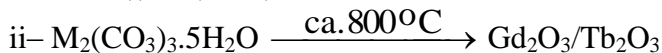
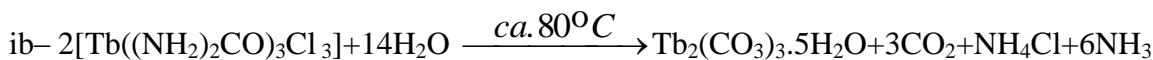
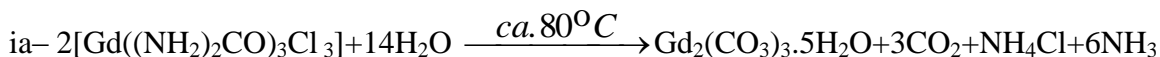
2.1. Reagents

Carbamide, $\text{GdCl}_3 \cdot 6\text{H}_2\text{O}$, $\text{TbCl}_3 \cdot 6\text{H}_2\text{O}$ and methanol solvent were obtained from Aldrich Company. Nalidixic acid drug was received from Fluka chemical company. All chemicals used in this study were of analytically reagent grade and used without further purification.

2.2. Synthesis of Gd(III) and Tb(III)–nalidixic acid complexes

2.2.1. Method of nano-particles preparation

The preparation can be summarized in four steps with sequence equations as follows;



The first step of preparation was discussed previously [26, 27] as follows: $\text{Ln}_2(\text{CO}_3)_3 \cdot 5\text{H}_2\text{O}$ (Ln = Gd and Tb(III)) were prepared by mixing aqueous solutions (100 ml) of 0.01 M of the respectively $\text{LnCl}_3 \cdot 6\text{H}_2\text{O}$ (Gd(III) or Tb(III)) with a volume of 100 ml of 0.1 M of carbamide. The mixtures were heated to *ca.* 80 °C for 2-4 h in a water bath. The precipitated white compounds were filtered out, washed several times with hot water, dried at *ca.* 80 °C in an oven for 2 h and then in *vacuo* over anhydrous calcium chloride. Carbonate contents in $\text{Ln}_2(\text{CO}_3)_3 \cdot n\text{H}_2\text{O}$ were determined by dissolving a weighted sample of the products in excess standard HCl and the excess of HCl was determined by titration with standard sodium carbonate. Lanthanide metal was determined gravimetrically as sesquioxides, Ln_2O_3 . The infrared spectra of carbamide and lanthanide carbonates were recorded in KBr discs. At room temperature, lanthanide(III) ions react with carbamide to form the complex, $\text{Ln}(\text{carbamide})_3\text{X}_3$ [28, 29]. The second step dealing the transfer of lanthanide(III) carbonates (Gd(III) and Tb(III)) constructed in the first step to form of nano-oxides particles, which have been examined using X-ray. In third step lanthanum(III) oxide was converted to its chloride by treating with concentrated hydrochloric acid. An aqueous solution of lanthanum chloride in fourth step was added to a mixed methanolic solution of NDX (the mole ratio ($\text{LnCl}_3 \cdot x\text{H}_2\text{O}$): (NDX) was 1:3), the pH value of which was adjusted to 8.0–9.0 by adding aqueous ammonia solution (5 %, V/V) with heating at 80–90 °C for about 4–5 h and continuous stirring. The precipitate was filtered off, washed with water and methanol, dried (90 °C), and then left over anhydrous calcium chloride.

2.3. Equipments

Elemental analyses of carbon, hydrogen and nitrogen elements were analyzed by a Perkin-Elmer CHN 2400 elemental analyzer. The metal contents were determined gravimetrically by converting the compounds to their corresponding oxides. The molar conductivities of freshly prepared $1.0 \times 10^{-3} \text{ mol/cm}^3$ dimethylsulfoxide solutions were measured for the soluble complexes using Jenway 4010 conductivity meter. The infrared spectra, as KBr discs, were recorded on a Bruker FT-IR Spectrophotometer (4000–400 cm^{-1}). The thermal studies were carried out on a Shimadzu thermo gravimetric analyzer at a heating rate of 10 °C min^{-1} under nitrogen till 800 °C. The X-ray diffraction patterns for the two lanthanide oxides were recorded on X'Pert PRO PAN analytical X-ray powder

diffraction, target copper with secondary monochromate. Scanning electron microscopy (SEM) images and Energy Dispersive X-ray Detection (EDX) were taken in Joel JSM-6390LA equipment, with an accelerating voltage of 20 KV.

2.4. Biological studies

Antimicrobial activity of the tested samples was determined using a modified Kirby-Bauer disc diffusion method [30]. Briefly, 100 μL of the best bacteria/fungi were grown in 10 mL of fresh media until they reached a count of approximately 10⁸ cells/mL for bacteria or 10⁵ cells/mL for fungi. 100 μL of microbial suspension was spread onto agar plates corresponding to the broth in which they were maintained. Isolated colonies of each organism that might be playing a pathogenic role should be selected from primary agar plates and tested for susceptibility by disc diffusion method. Of the many media available, National Committee for Clinical Laboratory Standards (NCCLS) recommends Mueller-Hinton agar due to: it results in good batch-to-batch reproducibility. Disc diffusion method for filamentous fungi tested by using approved standard method (M38-A) developed by the NCCLS for evaluating the susceptibility of filamentous fungi to antifungal agents [31-37]. Disc diffusion method for yeast developed standard method (M44-P) by the NCCLS. Plates inoculated with filamentous fungi as *Aspergillus Flavus* at 25 °C for 48 hours; Gram (+) bacteria as *Staphylococcus Aureus*, *Bacillus subtilis*; Gram (-) bacteria as *Escherichia Coli*, *Pseudomonas aeruginosa* they were incubated at 35-37 °C for 24-48 hours and yeast as *Candida Albicans* incubated at 30 °C for 24-48 hours and, then the diameters of the inhibition zones were measured in millimeters. Standard discs of Tetracycline (Antibacterial agent), Amphotericin B (Antifungal agent) served as positive controls for antimicrobial activity but filter disc impregnated with 10 μL of solvent (distilled water, DMSO) were used as a negative control. The agar used is Mueller-Hinton agar that is rigorously tested for composition and pH. Further the depth of the agar in the plate is a factor to be considered in the disc diffusion method [31-37]. This method is well documented and standard zones of inhibition have been determined for susceptible values. Blank paper disks (Schleicher & Schuell, Spain) with a diameter of 8.0 mm were impregnated 10 μL of tested concentration of the stock solutions. When a filter paper disc impregnated with a tested chemical is placed on agar the chemical will diffuse from the disc into the agar. This diffusion will place the chemical in the agar only around the disc. The solubility of the chemical and its molecular size will determine the size of the area of chemical infiltration around the disc. If an organism is placed on the agar it will not grow in the area around the disc if it is susceptible to the chemical. This area of no growth around the disc is known as a "Zone of inhibition" or "Clear zone". For the disc diffusion, the zone diameters were measured with slipping calipers of the National for Clinical Laboratory Standards [32-35]. Agar-based methods such as E-test disk diffusion can be good alternatives because they are simpler and faster than broth methods.

3. RESULTS AND DISCUSSION

The interactions of nalidixic acid with the two lanthanide(III) metal ions Gd(III) and Tb(III) gave a white solid complexes in acceptable yields (60–70%). The micro analytical and physical

measurements like percentage of (carbon, hydrogen and nitrogen) and decomposition temperatures of the compounds are presented in Table 1. The experimental and theoretical percentages of elemental analysis are in a good agreement with each other and supported the suggested molecular formula of the synthesized nalidixic acid complexes. The complexes have high thermal decomposition points above > 250 °C. The nalidixic acid ligand behaves as bidentate ligand and coordinated to the Gd(III) and Tb(III) metal ions via one carboxylate oxygen atom and the oxygen atom of the pyridine carbonyl group. The solid NDX complexes are 1:3 molar ratio of (Gd/Tb(III): NDX).

3.1. Molar conductivities

The molar conductance data has a supporting item, that been used in speculate the conformational structure of metal chelates. The measurement of conductance in solution form gave an idea about the degree of ionization (ions that liberated in solutions) for the resulted complexes. The higher data of molar conductivity is due to the presence of compound in electrolytic case and vice versa [38]. The molar conductivity values for the Gd(III) and Tb(III) complexes of nalidixic acid in DMSO solvent (1.00×10^{-3} M) were found to be in the range $19\text{--}22 \Omega^{-1} \cdot \text{cm}^2 \cdot \text{mol}^{-1}$ at room temperature, suggesting them to be non-electrolytes [39]. Hence the molar conductance values indicate that no ions are present outside the coordination sphere so that chloride ions may be exhibit inside the coordination sphere or absent. The obtained results were strongly matched with the elemental analysis data where Cl^- ions are absence in case of both Gd(III) and Tb(III) complexes after checked of these complexes using silver nitrate precipitated reagent. The above complexes are air-stable, insoluble in water, and soluble in dimethylsulfoxide, DMSO or dimethylformamide, DMF and concentrated mineral acids.

Table 1. Micro analytical and physical data of Gd(III) and Tb(III)/NDX complexes

Complexes Formula (Mwt)	(Calcd)/Found				Molar conductance/ $\Omega^{-1} \cdot \text{cm}^2 \cdot \text{mol}^{-1}$	Meltin g point/ °C
	%/C	%/H	%/N	%/M		
[Gd(NDX) ₃].6H ₂ O	(45.09) 44.89	(4.73) 4.33	(8.76) 8.59	(16.40) 16.32	22	>250
[Tb(NDX) ₃].6H ₂ O	(45.01) 44.81	(4.72) 4.55	(8.75) 8.64	(16.54) 16.21	19	>250

3.2. Electronic absorption spectra

The synthesized Gd(III) and Tb(III)/NDX complexes were also confirmed by electronic UV-vis spectra. Figure 2, show the electronic absorption spectra of the Gd(III) and Tb(III) complexes in DMSO within 200–600 nm range. The free nalidixic acid has two distinguish absorption bands at 254 and 356 nm which assigned to $\pi \rightarrow \pi^*$ and $n \rightarrow \pi^*$ transitions, respectively [40]. These transitions are existed in case of unsaturated hydrocarbons, which contain carbon atom attached with oxygen atoms as

in carboxylic and ketone groups [41]. These two bands of free NDX are hypsochromically affected in the electronic spectra of Gd(III) and Tb(III) complexes. The Gd(III) and Tb(III)/NDX complexes show two absorption bands at (240 and 330) nm and (250 and 305) nm, respectively, due to $\pi \rightarrow \pi^*$ and $n \rightarrow \pi^*$ transitions. The hypsochromically change in the spectra of both NDX complexes supported that the carboxylic group and ketone groups are involved in the coordination. Also, these results are compatible with the interpretations of FT-IR and $^1\text{H-NMR}$ spectra.

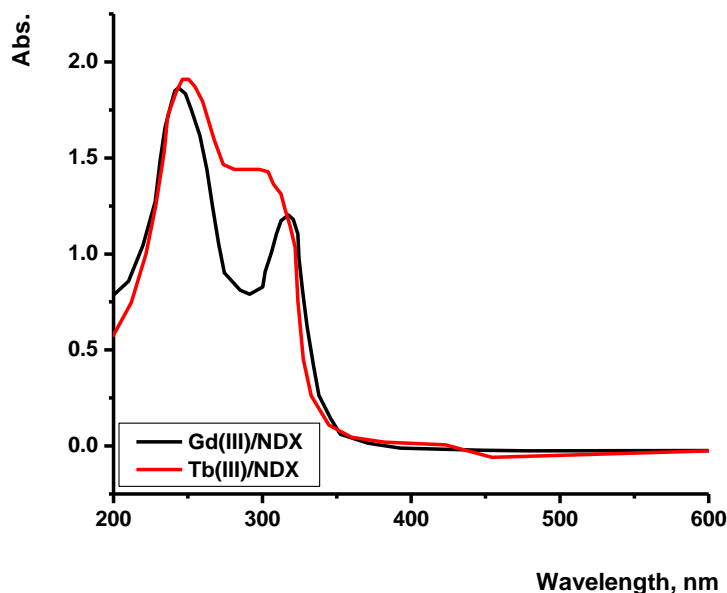


Figure 2. Electronic spectra of Gd(III) and Tb(III)/NDX complexes

3.3. Infrared spectra

In the comparison between infrared spectra of the synthesized Gd(III) and Tb(III) complexes (Fig. 3) with that of the free NDX ligand, the place of coordination for the NDX ligand with both metal ions have been discussed and summarized in Table 2. The free NDX ligand has a strong band located at 1717 cm^{-1} which assigned to the stretching vibration of the carbonyl $\nu(\text{CO})$ group for carboxylic $\nu(\text{COOH})$ [42]. Insight into the spectrum of NDX, it was found that the absence of the ν_{COOH} stretching vibration, explains strongly the deprotonation of NDX ligand [43]. In the literature survey [42] a study which deals with the location of both asymmetric (1570 cm^{-1}) and symmetric (1350 cm^{-1}) stretching depending upon the deprotonation of carboxylate group. The main infrared spectral bands detectable for the NDX ligand in the prepared complexes (Table 2) confirm the deprotonation case for the NDX complexes. In the coordination process, the carbonyl $\nu(\text{CO})$ group was absence and the $\nu(\text{COOH})$ stretching vibration in NDX ligand appeared at (1573 and 1577) cm^{-1} and (1353 and 1358) cm^{-1} due to the asymmetric and symmetric stretching vibration of the coordinated of COO^- group, respectively [42, 43]. It is well known that the carboxylate group has three types of coordination (unidentate, bidentate or bridge), then the basis of these knowledge can be said that unidentate

chelation take place when the difference in frequencies between asymmetric and symmetric stretching vibrations [$\Delta\nu = (\nu_{\text{asym}} \text{COO}^- - \nu_{\text{sym}} \text{COO}^-) \geq 200$] [42-44]. From the infrared spectra of both Gd(III) and Tb(III) complexes the calculated $\Delta\nu$ was observed at 219 and 215 cm^{-1} , respectively, which suggests a unidentate interaction of the carboxylate group toward the central metal ions in both NDX complexes. The other reason, which confirms the place of coordination is that the carbonyl group $\nu(\text{C}=\text{O})$ which presence at 1717 cm^{-1} for the free NDX was blue shifted by $\Delta\nu = 96$ and 77 cm^{-1} for Gd(III) and Tb(III)/NDX complexes, respectively. This discussion is strengthen the involvement of the carbonyl group in coordination of Gd(III) and Tb(III) complexes. The new band was involved in both Gd(III) and Tb(III) complexes at 451-622 cm^{-1} assigned to M-O stretching vibration motion [42, 44]. The uncoordinated water molecules in the Gd(III) and Tb(III) complexes were observed at the ~ 3400 -3200 cm^{-1} . From the above discussion we can say that, NDX ligand coordinated with Gd(III) and Tb(III) ions via two oxygen atoms of the carboxylate and the carbonyl groups, the most probable six coordinated fashion around each metal ion (Fig. 3) as designed below.

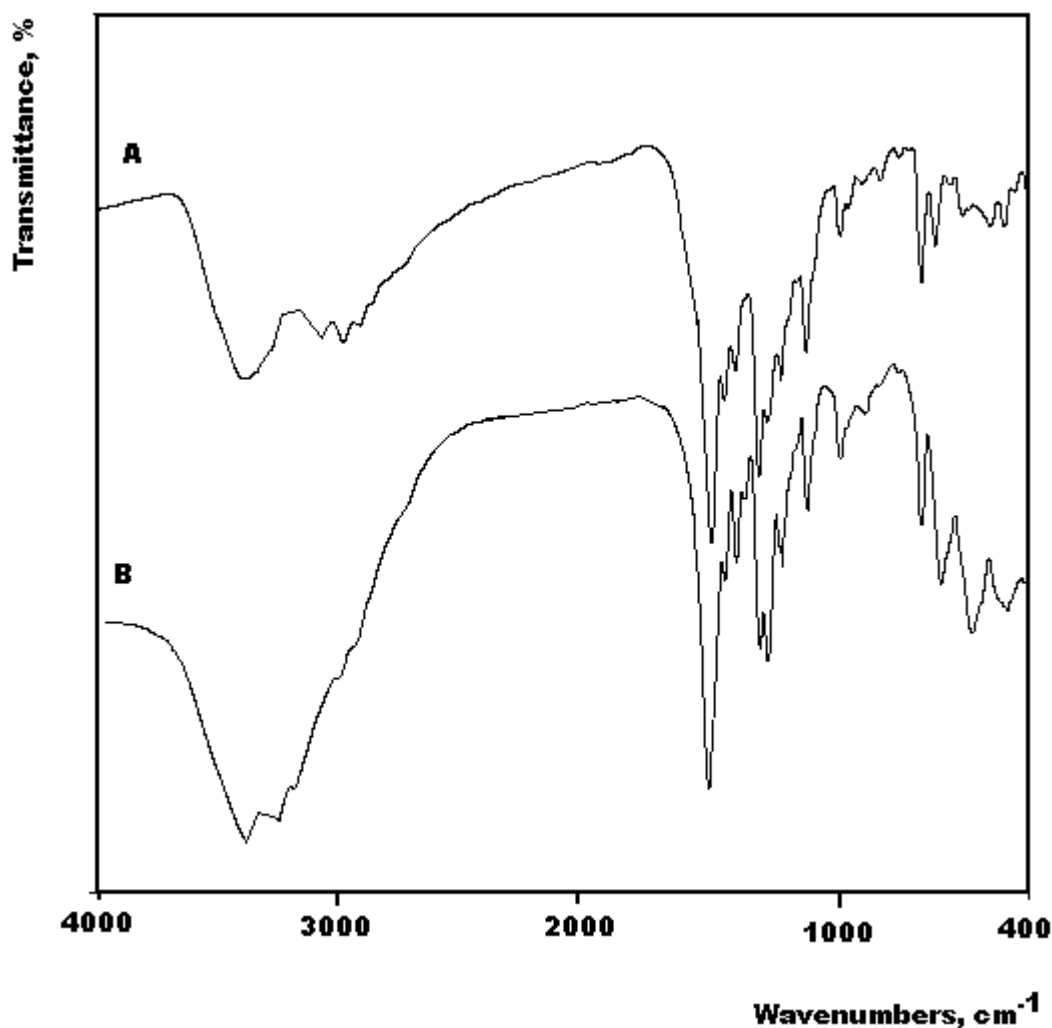
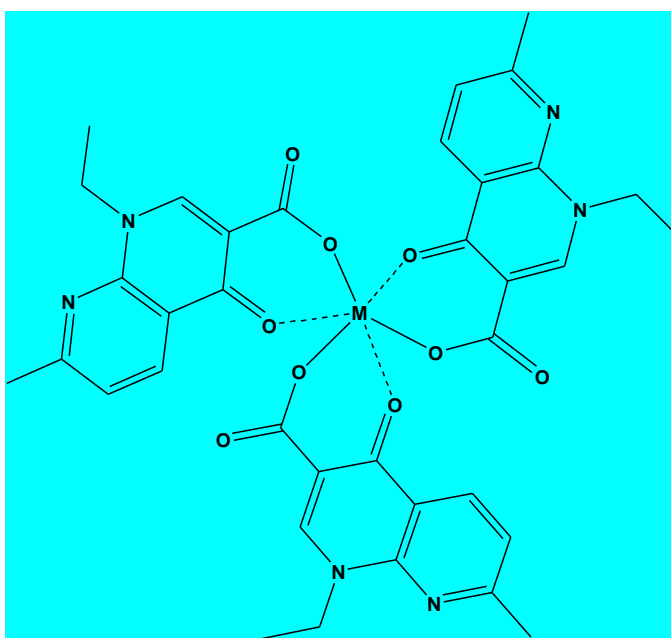


Figure 3. Infrared spectra of (A): Gd(III) and (B): Tb(III)/NDX complexes

Table 2. Distinguish infrared bands of NDX and their complexes.

Compound	$\nu(\text{C}=\text{O})$	$\nu(\text{COO})$ (asym)	$\nu(\text{COO})$ (sym.)	Δ $\nu(\text{asy.}-\text{sym.})$	$\nu(\text{M}-\text{O})$
NDX	1717	1616	1386	230	---
$[\text{Gd}(\text{NDX})_3] \cdot 6\text{H}_2\text{O}$	1620	1570	1351	219	546, 451
$[\text{Tb}(\text{NDX})_3] \cdot 6\text{H}_2\text{O}$	1640	1575	1360	215	522, 487

**Figure 4.** Suggestion structure of $[\text{M}(\text{NDX})_3] \cdot 6\text{H}_2\text{O}$ complexes (where, $\text{M} = \text{Gd}(\text{III})$ or $\text{Tb}(\text{III})$)

3.4. $^1\text{H-NMR}$ spectra

The $^1\text{H-NMR}$ data of the free nalidixic acid and its $\text{Gd}(\text{III})$ complex as an example were discussed. The characteristic peaks of NDX free ligand can be summarized as: 14.870 ppm (H; COOH), 9.174 ppm (H; $\text{C}=\text{H}$), 8.602 ppm (H; pyridine ring), 7.596 ppm (H; pyridine ring), 4.640 ppm (2H; CH_2CH_3), 2.712 ppm (3H; CH_3 -pyridine ring) and 1.425 ppm (3H; CH_2CH_3). Through the comparison with the free NDX ligand, the absence of the characteristic peak for hydrogen of $-\text{COOH}$ at $\delta = 14.870$ ppm in $\text{Gd}(\text{III})$ complex indicates that the coordination of NDX ligand to $\text{Gd}(\text{III})$ occur through the deprotonated carboxylic group [41]. The proton NMR spectrum for $\text{Gd}(\text{III})$ complex show peaks at the range of (3.30 - 3.50) ppm, this peaks aren't observed in the free NDX ligand spectrum and can be assigned to the protons of H_2O molecules, supporting the complex formula. The overall changes of the $^1\text{H-NMR}$ spectrum of the $\text{Gd}(\text{III})$ complexes are indicative of coordination of NDX ligand to the metal ions via the pyridone and one carboxylate oxygen atoms [45].

3.5. Thermal analysis

The well-established thermogravimetric analysis (TGA) and differential scanning calorimetry (DSC) techniques have been reliably widely used over many decades in studying the thermal behavior and properties of various types of materials and evaluating the parameters for their degradation processes. These methods have allowed determination of the chemical steps of the investigated degradation and the evaluation, by some methods [46-52], of the kinetic parameters for each step. The evaluation of the kinetic parameters has been performed by using a thermogravimetric curve (TG curve) recorded at a certain heating rate and atmospheres (under nitrogen or air flow).

The obtained Gd(III) and Tb(III) NDX complexes were studied by thermo gravimetric and its differential analysis (TG/DTG/DTA) from ambient temperature to 800 °C under N₂ atmospheres. The TG curves were redrawn as mg mass loss versus temperature and DTG curves were redrawn as rate of loss of mass versus temperature. The thermal decomposition curves (TG/DTG/DTA) are given in Figs. (5-6).

3.5.1. [Gd(NDX)₃].6H₂O complex

Thermal decomposition of Gd(III)/NDX complex with general formula [Gd(NDX)₃].6H₂O occurs at six steps. The first decomposition step take place at a temperature range of 35-120 °C at DTG_{max}=86 °C and it correspond to the loss of one of hydrated water molecule with an observed weight loss 2.00% (calcd.=1.88%). The second step occur within a temperature range 120-290 °C at DTG_{max}=144, 222 °C which assigned to the loss of five molecule of hydration water + three 3-methyl-pyridine molecules with a weight loss (obs.= 39.00%, calcd.= 38.52%). The third-six steps occur within a temperature range 290-800 °C at DTG_{max}= (302, 571 and 605) °C and DTA= (570 and 601) °C (exo) which assigned to the decomposition of ethyl-pyridin-4-one carboxylic acid organic moiety with a weight loss (obs.= 40.00%, calcd.= 40.70%). The ½Gd₂O₃ is the final product remains stable till 800 °C as final residual with mass percentage (obs= 19.00%, calcd.= 18.90%).

3.5.2. [Tb(NDX)₃].6H₂O complex

The thermal decomposition of Tb(III)/NDX complex with the general formula [Gd(NDX)₃].6H₂O occurs at consecutive and very evenly seven steps. The first decomposition step presence at a temperature range of 30-70 °C at DTG_{max}= 75 °C and it correspond to the loss of 2H₂O hydrated molecules with an observed weight loss 3.50% (calcd.= 3.75%). The second step occur within a temperature range 70-180 °C at DTG_{max}= 176 °C and DTA=216 °C which assigned to the loss of 5H₂O hydrated water molecules + three terminal ethyl groups of the ethyl-pyridin-4-one carboxylic acid organic moiety with a weight loss (obs.=16.00%, calcd.=16.24%). The third-to-seven degradation steps occur within a temperature range 180-800 °C at DTG_{max} = (276, 336, 439, 568 and 765) °C and DTA= (274(endo), 324(endo), 378(endo), 501(exo) and 564(exo)) °C which assigned to the thermal decomposition of loss of both three 3-methyl-pyridine and three pyridin-4-one carboxylic acid main moieties of NDX ligand with a weight loss (obs.= 59.86%, calcd.= 61.04%). The ½Tb₂O₃ is the final

product remains stable till 800 °C as final residual with mass percentage (obs= 19.04%, calcd.= 18.97%).

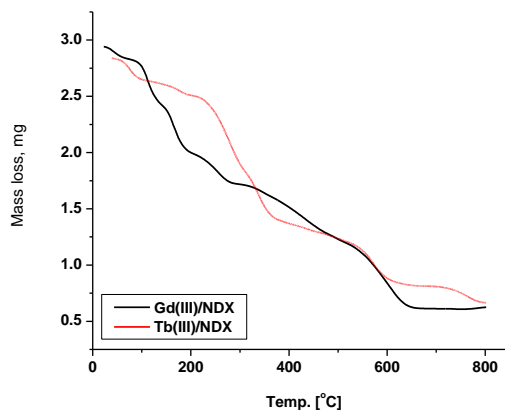


Figure 5. TG curves of Gd(III) and Tb(III)/NDX complexes

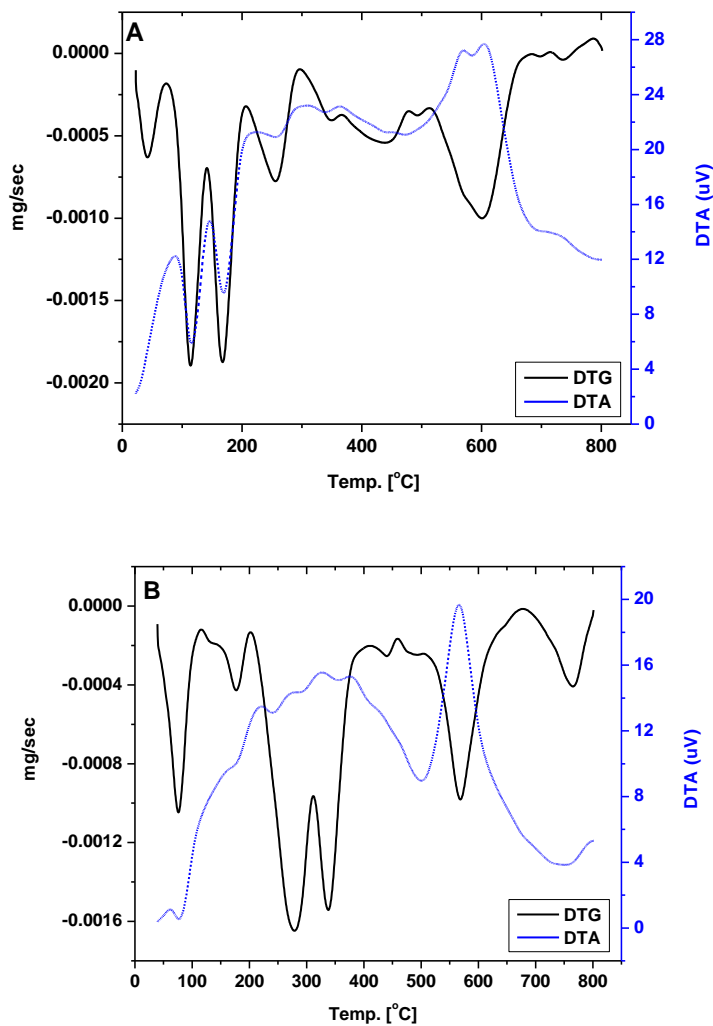


Figure 6. DTG/DTA curves of (A): Gd(III) and (B): Tb(III)/NDX complexes

3.6. Kinetic studies

The determination of the rate-dependent parameters of solid-state non-isothermal decomposition reactions were operated using analysis of TG curves [46-52]. Most commonly used methods are the differential method of Freeman and Carroll [46] integral method of Coat and Redfern [47] and the approximation method of Horowitz and Metzger [50]. In the present paper, the general thermal behaviors of the Gd(III)/Tb(III)-NDX complexes in terms of stability ranges, peak temperatures and values of kinetic parameters are discussed. The kinetic parameters have been evaluated using the Coats-Redfern equation:

$$\int_0^\alpha \frac{d\alpha}{(1-\alpha)^n} = \frac{A}{\varphi} \int_{T_1}^{T_2} \exp\left(-\frac{E^*}{RT}\right) dt \quad (\text{eq. 1})$$

This equation on integration gives;

$$\ln\left[-\frac{\ln(1-\alpha)}{T^2}\right] = -\frac{E^*}{RT} + \ln\left[\frac{AR}{\varphi E^*}\right] \quad (\text{eq. 2})$$

A plot of left-hand side (LHS) against $1/T$ was drawn. E^* is the energy of activation in J mol^{-1} and calculated from the slop and A in (s^{-1}) from the intercept value. The entropy of activation ΔS^* in $(\text{JK}^{-1}\text{mol}^{-1})$ was calculated by using the equation:

$$\Delta S^* = R \ln(Ah/k_B T_s) \quad (\text{eq. 3})$$

Where k_B is the Boltzmann constant, h is the Plank's constant and T_s is the DTG peak temperature [52].

The Horowitz-Metzger equation is an illustrative of the approximation methods.

$$\log\left[\frac{1-(1-\alpha)^{1-n}}{(1-n)}\right] = E^* \theta / 2.303RT_s^2 \quad \text{for } n \neq 1 \quad (\text{eq. 4})$$

When $n = 1$, the LHS of equation 4 would be $\log[-\log(1-\alpha)]$. For a first-order kinetic process the Horowitz-Metzger equation may be written in the form:

$$\log[\log(w_\alpha / w_\gamma)] = E^* \theta / 2.303RT_s^2 - \log 2.303 \quad (\text{eq. 5})$$

Where $\theta = T - T_s$, $w_\gamma = w_\alpha - w$, w_α = mass loss at the completion of the reaction; w = mass loss up to time t . The plot of $\log[\log(w_\alpha / w_\gamma)]$ vs θ was drawn and found to be linear from the slope of which E^* was calculated. The pre-exponential factor, A , was calculated from the equation:

$$E^* / RT_s^2 = A / [\varphi \exp(-E^*/RT_s)] \quad (\text{eq. 6})$$

The entropy of activation, ΔS^* , was calculated from equation 3. The enthalpy activation, ΔH^* , and Gibbs free energy, ΔG^* , were calculated from;

$$\Delta H^* = E^* - RT \quad \text{and} \quad \Delta G^* = \Delta H^* - T\Delta S^* \quad (\text{eq. 7})$$

Herein, the thermal behaviors of the nalidixic acid complexes in terms of stability ranges, peak temperatures and values of kinetic parameters, are shown in Table 3 and Figs. 7-8. The kinetic parameters have been evaluated using the Coats-Redfern and Horowitz-Metzger equations. From the kinetic and thermodynamic data resulted from the TGA curves and tabulated in Table 3, the following outcome can be discussed as follows:

- The higher values of activation energies of the NDX complexes led to thermal stability of the studied complexes.
- The thermodynamic data obtained with the two methods are in harmony with each other. The correlation coefficients of the Arrhenius plots of the thermal decomposition steps were found to lie in the range $\sim 0.98-0.99$, showing a good fit with linear function.

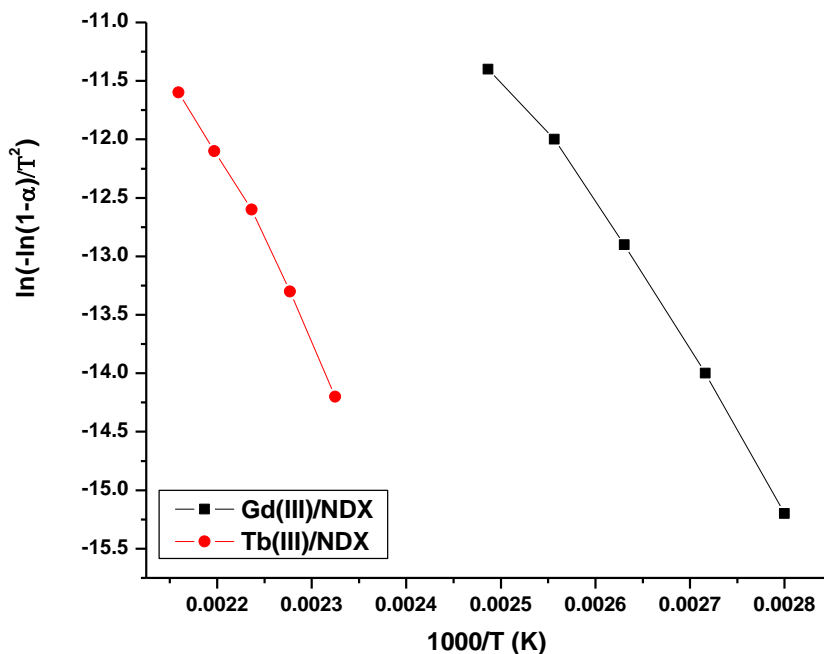


Figure 7. Plots of Coats–Redfern (CR) relation for Gd(III) and Tb(III)/NDX complexes

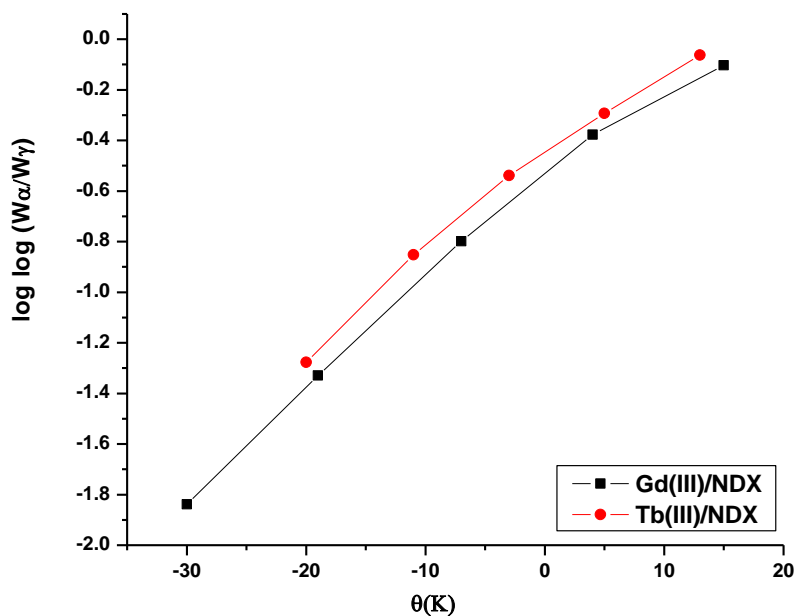


Figure 8. Plots of Horowitz–Metzger (HM) relation for Gd(III) and Tb(III)/NDX complexes

- It is clear that the thermal decomposition process of most NDX complexes is non-spontaneous ($\Delta S^* = \text{negative value}$), i.e., the complexes are thermally stable.
- The thermograms and the calculated thermal parameters for the NDX complexes show that the stability of these complexes depends on the nature of the central metal ion.

- The values of activation energy of the second stages of decomposition are found to be higher than that of the first stages, while that of the third stage are found to be higher than that of the second stage and so. This may indicate that the rate of decomposition of the second stage is lower than that of the first stage, whereas that of the third stage is lower than that of the second stage. This may be attributed to the structural rigidity of the ligand as compared with H₂O and methyl groups, which requires more energy for its rearrangement before undergoing any compositional change.

Table 3. Kinetic parameters using the Coats–Redfern (CR) and Horowitz–Metzger (HM) equations for the Gd(III) and Tb(III)/NDX complexes

Complex	Method	Parameter					r
		E (J mol ⁻¹)	A (s ⁻¹)	ΔS (J mol ⁻¹ K ⁻¹)	ΔH (J mol ⁻¹)	ΔG (J mol ⁻¹)	
Gd(III)	CR	7.00E+04	2.81E+08	-8.50E+01	6.78E+04	9.50E+04	0.9921
	HM	7.10E+04	4.23E+09	-6.22E+01	7.10E+04	9.21E+04	0.9861
Tb(III)	CR	5.12E+04	5.30E+04	-1.61E+02	4.77E+04	1.00E+05	0.9902
	HM	5.45E+04	4.62E+05	-1.44E+02	5.30E+04	1.02E+05	0.9861

r = correlation coefficient of the linear plot.

3.7. XRD and SEM studies

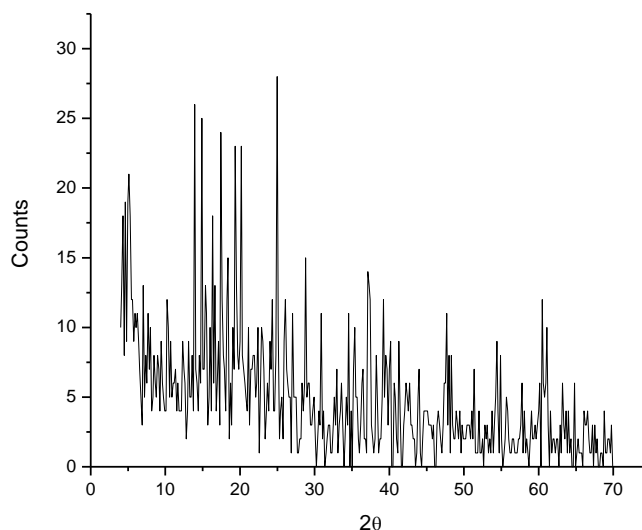


Figure 9. The XRD spectrum of Gd₂O₃.

The x-ray powder diffraction patterns (Fig. 9) in the range of 20° < 2θ < 70° for the residual products of thermal decomposition at 800 °C which resulted from the interaction between GdCl₃ or TbCl₃ with carbamide were carried in order to obtain an idea about the lattice dynamics of the resulted oxides of Gd(III) and Tb(III). For example the values of 2θ, full width at half maximum (FWHM) of

prominent intensity peak, relative intensity and particle size of Gd(III) oxide as a residual product have 24° , 0.2475, 100 and 6 nm, respectively. The crystallite size of the Gd(III) oxide could be estimated from XRD patterns by applying FWHM of the characteristic peaks using Deby-Scherrer equation 8 [53].

$$D = K\lambda / \beta \cos\theta \quad (\text{eq. 8})$$

Where D is the particle size of the crystal gain, K is a constant (0.94 for Cu grid), λ is the x-ray wavelength (1.5406 Å), θ is the Bragg diffraction angle and β is the integral peak width. The particle size was estimated according to the highest value of intensity compared with the other peaks. The particle size for the Gd(III) thus obtained was 6.0 nm. These data gave an impression that the particle size located within nano scale range.

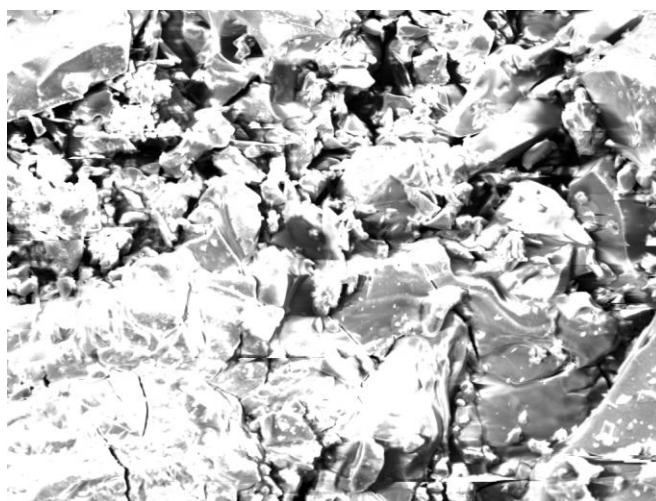


Figure 10. SEM images of Gd(III)/NDX complexes synthetic by un-conventional method.

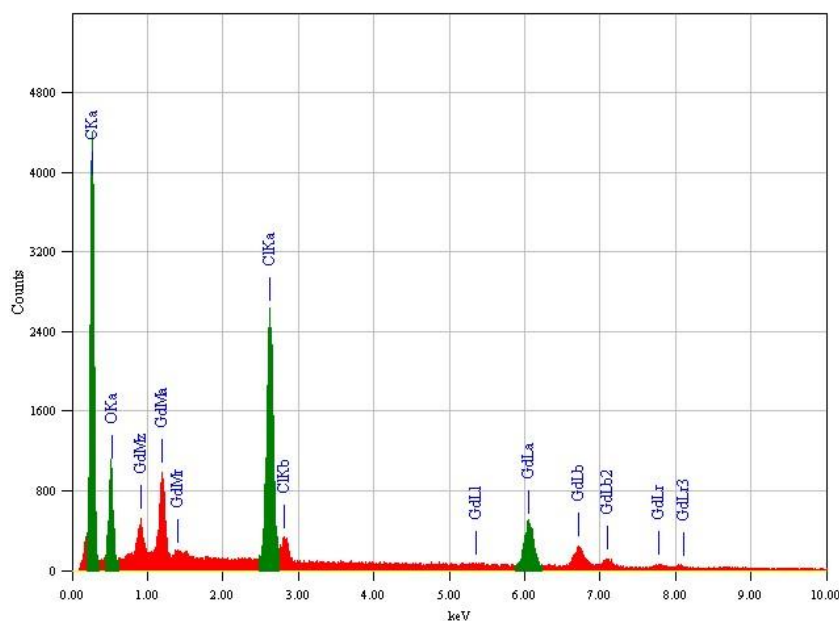


Figure 11. EDX images of Gd(III)/NDX complexes synthetic by un-conventional method.

Scanning electron microscopy is a simple tool used to give an impression about the microscopic aspects of the physical behavior of the Gd(III)/NDX complex formation (Fig. 10). Energy Dispersive X-ray Detection (Fig. 11) was also operated to check the elements which consist of gadolinium(III) oxide resulted from the second step for the method of nano-particles preparation. Although this tool is not a qualified method to confirm complex formation but it can be a reference to the presence of a single component in the synthetic products.

3.8. Microbiological investigation

Regarding the inhibition zone diameter, Gd(III)/Tb(III)-NDX complex in nano scale has highest antimicrobial activity against all target organisms compared to other which prepared by traditional methods (Fig. 12). Also, Gd(III)/Tb(III)/NDX compounds in nano range gained approximately twice percentage rather than traditional method of preparation in comparable with antibacterial agent (Tetracycline) and antifungal agent (Amphotericin B). The most reasons for lethal action of tested compounds may due to their interactions with critical intracellular sites causing the death of cells [54]. The variety of antimicrobial activities of tested compounds may due to a different degree of tested compounds penetration through cell membrane structure of target organism. In conclusion, the interactions between the gadolinium(III) and terbium(III) ions in nano-structural form resulting developing of the effectiveness of biological characters of Gd(III) and Tb(III) ions antibiotics.

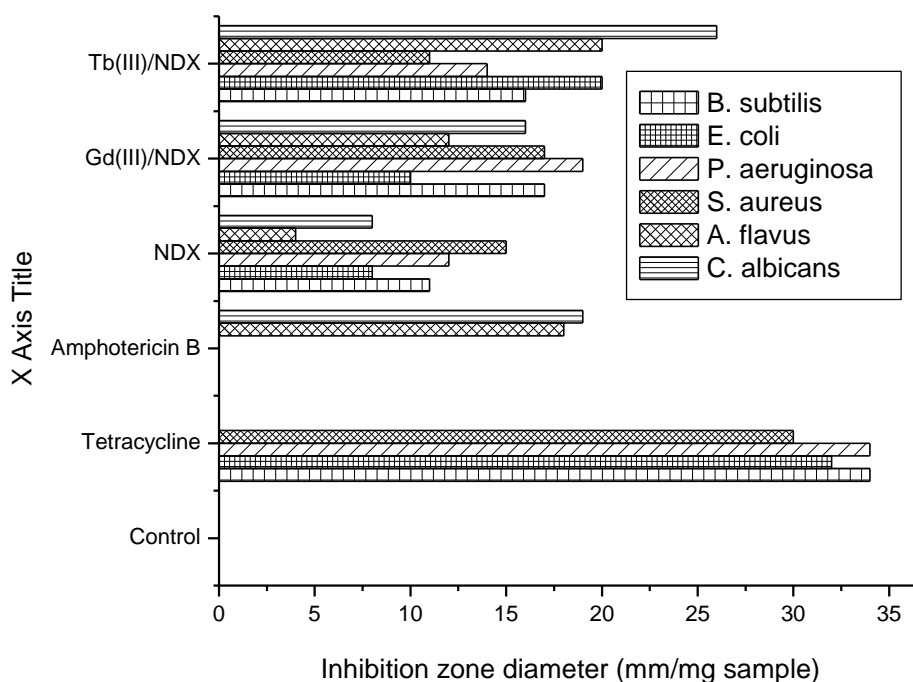


Figure 12. Diagram of inhibition zone diameter (mm) of the target compounds against tested microorganisms.

References

1. A. Albert, *The Physico-Chemical Basis of Therapy: Selective Toxicity*, 6th ed., Chapman & Hall, London, (1979).
2. M.N. Hughes (Ed.), *The Inorganic Chemistry of Biological Processes*, 2nd ed., Wiley, New York, (1981).
3. J. Liu, E.B. Wang, J. Peng, and Y.S. Zhou, *J. Rare Earths*, 17, (1999) 139.
4. S. Chakrabarti, D. Dasgupta and D. Bhattacharyya, *J. Biol. Phys.*, 26, (2000) 203.
5. G.A. Smita, Ranjit and V. Vikrant, *International J. Pharm. Res. Development*, 3, (2011) 164-171.
6. A.R. Shaikh, R. Giridhar, and M.R. Yadav, *International J. Pharmaceutics*, 332 (2007) 24-30.
7. I. Turel, The interaction of metal ions with quinolone antibacterial agents. *Coord. Chem. Reviews*, 232 (2002) 27-47.
8. G Psomas, T. Alketa K. E. Efthimiadou, S. Yiannis, P. R Catherine and K. Nikos, *J. Inorg. Biochem.*, 100 (2006) 1764-1773.
9. E.K. Efthimiadou, T. Hellinida, S. Yiannis, C. P. Raptopoulou and A. S. Katsaros, Alexandra Karaliota, George Psomas, *J. Inorg. Biochem.*, 101, (2007) 64-73.
10. E. K. Efthimiadou and K. Alexandra, P. George, *Polyhedron*, 27 (2008) 1729-1738.
11. A. Kumar and S.Y. Danveer, *Int. J. Chem. Sci.*, 7(1) (2009)7-19.
12. K.C. Skyrianou, V. Psycharis, C.P. Raptopoulou, D.P. Kessissoglou, and G. Psomas, *J. Inorg. Biochem.*, 105 (2011) 63-74.
13. A.M.A. Adam, *J. Mat. Sci. Res.*, 1 (2012).
14. P. Živec, P. Franc, T.G. Iztok, P. Gerald, P. George, *J. Inorg. Biochem.*, 117 (2012) 35-47.
15. M. A. Marianthi, G. Andreadou P. R, Catherine. Psycharis, Anastasia A. Pantazaki, George Psomas, *J. Inorg. Biochem.*, 121 (2013) 88-99.
16. M.N.Patel, R. P. Chintan, N. J. Hardik, *Inorg. Chem. Commun.*, 27 (2013) 51-55
17. D.E King., R. Malone and, S.H. Lilley, *Am. Fam. Physician*, 61(2000) 2741-2748.
18. V.T. Andriole, (Ed.), *The Quinolones*, 3rd Ed, Academic Press, San Diego, (2000).
19. G.Y. Leshner, and M.D. Gruett, *Belg. Pat.*, (1962) 612 258.
20. E. Ruzicka, J. Lasovsky and P. Brazdil, *Chem. Zvesti*, 29 (1975) 517.
21. K. Timmers, R. Sternglanz, *Bioinorg. Chem.*, 9 (1978) 145.
22. M. Nakano, M. Yamamoto and T. Arita, *Chem. Pharm. Bull.*, 26 (19781) 1505.
23. W.R. Vicent, S.G. Schulman, J.M. Midgley, W. J. Van Ort and R.H.A. Sorel, *Int. J. Pharm.*, 9 (1981) 191.
24. S. Panadero, A.H. Gómez and D.B. Pérez, *Anal. Chim. Acta*, 303 (1995) 39.
25. J. Kljun, A.K. Bytzek, W. Kandioller, C. Bartel, M.A. Jakupec, C.G. Hartinger, B.K. Keppler and I. Turel, *Organometallics*, 30 (2011) 2506.
26. M.S. Refat, *Synth. React. Inorg. Met.-Org. Chem.*, 34(9) (2004) 1605.
27. S.M. Teleb and M.S. Refat, *Bull. Chem. Tech. Maced.*, 25(1) (2006) 57.
28. Yu. Ya. Kharitonov, K.S. Sulaimankulov and N.B. Khudaibergenova, *Zh. Neorg. Khim.*, 35 (8) (1990) 2117.
29. C.V. Deshpande and V.R. Rao, *J. Indian Inst. Sci.*, 69(5) (1989) 329.
30. A.W. Bauer, W.M. Kirby, C. Sherris and M. Turck, *Amer. J. Clinical Pathology*, 45 (1966) 493.
31. M.A. Pfaller, L. Burmeister, M.A. Bartlett and M.G. Rinaldi, *J. Clin. Microbiol.* 26 (1988) 1437.
32. National Committee for Clinical Laboratory Standards, Performance Vol. antimicrobial susceptibility of Flavobacteria, (1997).
33. National Committee for Clinical Laboratory Standards. 1993. Methods for dilution antimicrobial susceptibility tests for bacteria that grow aerobically. Approved standard M7-A3. National Committee for Clinical Laboratory Standards, Villanova, Pa.

34. National Committee for Clinical Laboratory Standards. (2002). Reference Method for Broth Dilution Antifungal Susceptibility Testing of Conidium-Forming Filamentous Fungi: Proposed Standard M38-A. NCCLS, Wayne, PA, USA.
35. National Committee for Clinical Laboratory Standards. (2003). Methods for Antifungal Disk Diffusion Susceptibility Testing of Yeast: Proposed Guideline M44-P. NCCLS, Wayne, PA, USA.
36. L.D. Liebowitz, H.R. Ashbee, E.G.V. Evans, Y. Chong, N. Mallatova, M. Zaidi, D. Gibbs, and Global Antifungal Surveillance Group. *Diagn. Microbiol. Infect. Dis*, 4 (2001) 27.
37. M.J. Matar, L. Ostrosky-Zeichner, V.L. Paetznick, J.R. Rodriguez, E. Chen, J.H. Rex, *Antimicrob. Agents Chemother.*, 47 (2003) 1647.
38. W.J. Geary, *Coord. Chem. Rev.*, 7 (1971) 81.
39. T. Vogel, *Textbook of Practical Organic Chemistry*. 4th Edn., John Wiley Inc., England, (1989) 133.
40. A.V. Polishchuk, E.T. Karaseva, T.B. Emelina, M.N. Yu and V.E. Karasev, *J. Stru. Chem.*, 50(3) (2009) 434.
41. M.S. Refat, *Spectrochimica Acta Part A*, 68 (2007) 1393.
42. I. Turel, I. Leban and N. Bukovec, *J. Inorg. Biochem.*, 66 (1997) 241.
43. G.B. Deacon and R.J. Phillips, *Coord. Chem. Rev.*, 33 (1980) 227.
44. I. Turel, L. Golic and O.L.R. Ramirez, *Acta Chem. Slov.*, 46(2) (1999) 203.
45. C.M. Riley, D.L. Ross, D. Van der Velde and F. Takusagawa, *J. Pharm. Biomed. Analysis*, 11 (1993) 49.
46. E.S. Freeman and B. Carroll, *J. Phys. Chem*, 62 (1958) 394.
47. A.W. Coats and J.P. Redfern, *Nature*, 201 (1964) 68.
48. T. Ozawa, *Bull. Chem. Sot. Jpn*, 38 (1965) 1881.
49. W.W. Wendlandt, *Thermal Methods of Analysis*, Wiley, New York, (1974).
50. H.W. Horowitz and G. Metzger, *Anal. Chem.*, 35 (1963) 1464.
51. J.H. Flynn, and L.A. Wall, *Polym. Lett.*, 4 (1966) 323.
52. P. Kofstad, *Nature*, 179 (1957) 1362.
53. C.X. Quan, L.H. Bin and G.G. Bang, *Mater. Chem. Phys.* 91 (2005) 317.
54. S.D. Cox, C.M. Mann, J.L. Markham, J.E. Gustafson, J.R. Warmington and S.G. Wyllie, *Molecules*, 6 (2001) 87.

© 2014 The Authors. Published by ESG (www.electrochemsci.org). This article is an open access article distributed under the terms and conditions of the Creative Commons Attribution license (<http://creativecommons.org/licenses/by/4.0/>).